ornl

ORNL/TM-7239

OAK
RIDGE
NATIONAL
LABORATORY

UNION
CARBIDE

Stress Relaxation and Creep of High-Temperature Gas-Cooled Reactor Core Support Ceramic Materials—A Literature Search

J. E. Selle
V. J. Tennery

OPERATED BY
UNION CARBIDE CORPORATION
FOR THE UNITED STATES
DEPARTMENT OF ENERGY

Printed in the United States of America Available from
National Technical Information Service
U.S. Department of Commerce
5285 Port Royal Road, Springfield, Virginia 22161
NTIS price codes—Printed Copy: A03; Microfiche A01

DISCLAIMER

ORNL/TM-7239
Distribution
Category UC-77

Contract No. W-7405-eng-26

METALS AND CERAMICS DIVISION

HTGR BASE TECHNOLOGY PROGRAM

Structural Materials Program (189a 01332)

STRESS RELAXATION AND CREEP OF HIGH-TEMPERATURE GAS-COOLED REACTOR CORE SUPPORT CERAMIC MATERIALS — A LITERATURE SEARCH

J. E. Selle and V. J. Tennery

Date Published - May 1980

OAK RIDGE NATIONAL LABORATORY
Oak Ridge, Tennessee 37830
operated by
UNION CARBIDE CORPORATION
for the
U.S. DEPARTMENT OF ENERGY

CONTENTS

ABSTRACT 1
INTRODUCTION 1
EXPERIMENTAL METHODS 8
  Sources of Error 11
  Stress Distribution 12
  Strain Measurements 13
SUMMARY OF EXPERIMENTAL WORK 14
  Creep 16
  Stress Relaxation 18
SUMMARY 18
ACKNOWLEDGMENTS 19
REFERENCES 19
APPENDIX 23

STRESS RELAXATION AND CREEP OF HIGH-TEMPERATURE GAS-COOLED REACTOR CORE SUPPORT CERAMIC MATERIALS — A LITERATURE SEARCH

J. E. Selle and V. J. Tennery

ABSTRACT

Creep and stress relaxation in structural ceramics are important properties to the high-temperature design and safety analysis of the core support structure of the High-Temperature Gas-Cooled Reactor (HTGR). The ability of the support structure to function for the lifetime of the reactor is directly related to the allowable creep strain and the ability of the structure to withstand thermal transients. The thermal-mechanical response of the core support pads to steady-state stresses and potential thermal transients depends on many variables, including the ability of the ceramics to undergo some stress relaxation in relatively short times.

An assessment of published work was made to examine creep and stress relaxation phenomona in structural ceramics of interest. Of the materials considered (fused silica, alumina, silicon nitride, and silicon carbide), alumina has been more extensively investigated in creep than the others. Activation energies reported varied between 482 and 837 kJ/mole, and consequently, variations in the assigned mechanisms were noted. Most investigators have designated Nabarro-Herring creep as the primary creep mechanism, although no definite grain size dependence has been identified. The results for silicon nitride are in better agreement with reported activation energies of 586 to 649 kJ/mole. No creep data were found for fused silica or silicon carbide and no stress relaxation data were found for any of the candidate materials.

While creep and stress relaxation are similar and it is theoretically possible to derive the value of one property when the other is known, no explicit demonstrated relationship exists between the two. We therefore conclude that for a given structural ceramic material, both properties must be experimentally determined to obtain the information necessary for use in high-temperature design and safety analyses.

INTRODUCTION

A structural ceramics program has been undertaken to provide information on the mechanical properties of candidate materials for use in a High-Temperature Gas-Cooled Reactor (HTGR). Specifically, these materials are structural ceramics required for core support pads, cover blocks, and helium duct liners. Schematics of the HTGR lower plenum thermal barrier and core support systems are shown in Figs. 1 and 2, respectively.

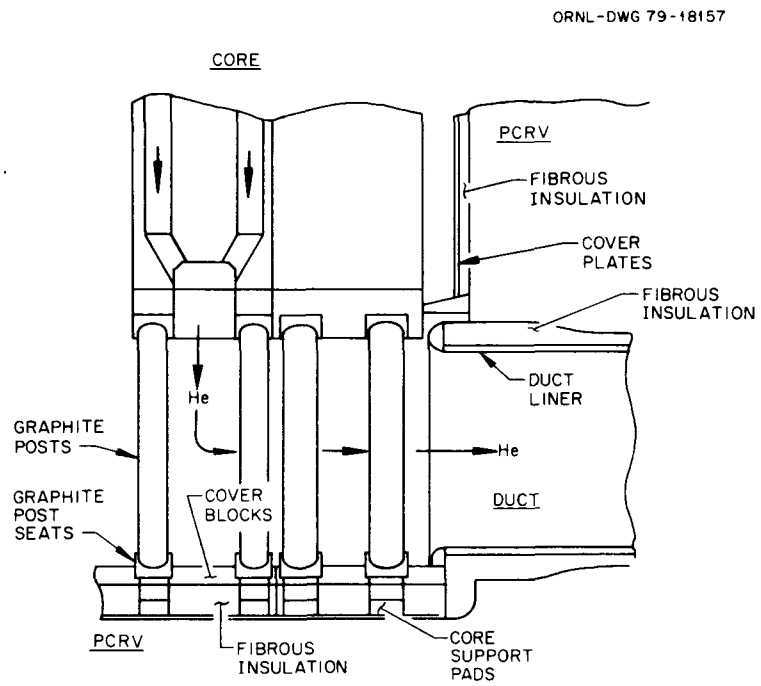

Fig. 1. Schematic of Reactor Lower Plenum Thermal Barrier.

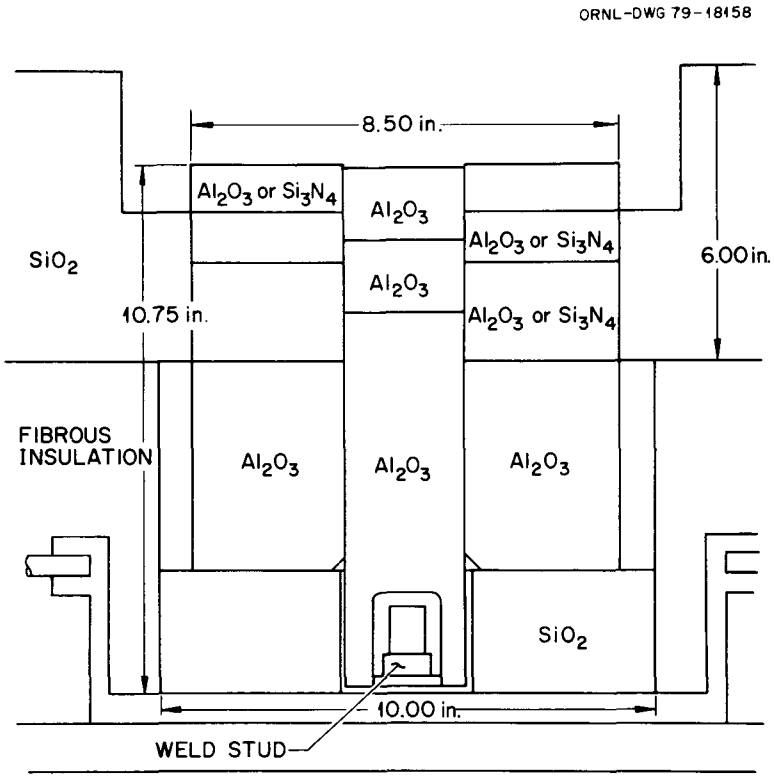

Fig. 2. Schematic of Core Support Pad Arrangement.

These figures also give an indication of the types of materials being considered for the various components. Table 1 summarizes these components and materials along with some of the service conditions of concern. The temperatures presented in this table should be regarded as approximate and therefore subject to change as the reactor design becomes finalized. The temperature ranges given indicate the temperature gradients across the components from top to bottom. These gradients also produce stresses in the materials and temperature excursions can increase these stresses.

Table 1. Service Conditions for Components in a Direct-Cycle HTGR

Application	Temperature Variation (°C)	Service Conditions	Candidate Materials
Upper pad	849–793	7.80 MPa He (77 atm) at 45.7 mps (150 fps) 2.76 MPa (400 psi) compressive stress plus thermal stresses	Al_2O_3, Si_3N_4
Second pad	793–735		Al_2O_3, Si_3N_4
Middle pad	735–621	7.8 MPa He (77 atm) at 45.7 mps (150 fps) 2.76MPa (400 psi) compressive stress plus thermal stresses	Al_2O_3, Si_3N_4
Fourth pad	621–477		Al_2O_3
Lower pad	477–66	7.8 MPa He (77 atm) at 45.7 mps (150 fps) 2.76 MPa (400 psi) compressive stress plus thermal stresses	Fused silica
Cover block	849–516	7.8 MPa He (77 atm) at 45.7 mps (150 fps) 0.7–1.03 MPa (100–150 psi) stresses plus thermal stresses	Fused silica, SiC, $SiON_2$, Si_3N_4
Hot duct liner	~850	0.35–0.7 MPa (50–100 psi) compressive stress plus thermal stresses plus vibrational stresses 91.4 mps (300 fps) helium velocity	C-C composites

Two pertinent properties particularly required for design of the core support structures are creep and stress relaxation of the relevant structural ceramics. The data base on these properties for the candidate materials is insufficient at the present time. When one examines the reported mechanisms of creep and stress relaxation in solids, it becomes apparent that the two are essentially relaxation phenomena and therefore one could possibly derive stress relaxation information from creep data or vice versa. In view of this possibility, we decided to review the literature to

summarize the state of the art on the subject, to identify similarities and differences, and to identify test procedures for determining these properties. Attention will be concentrated on ceramic materials, since these are the materials of interest due to the temperatures and stresses in this application.

Creep is the slow deformation that occurs in materials at high temperature and constant stress, while stress relaxation is the relief or change of stress required to maintain a constant strain. Mechanisms of both phenomena rely on atom movements. However, creep tests usually measure the strain at constant stress while stress relaxation tests measure the stress variation at constant strain. Figure 3 compares these two phenomena at low temperatures and stresses. Both of these properties can be modeled mathematically by the so-called "standard linear solid,"[1] two equivalent models of which are shown in Fig. 4. Both of these models yield the same differential stress-strain equations. However, the Voight-type model [Fig. 4(a)] is more convenient for analyzing creep behavior, while

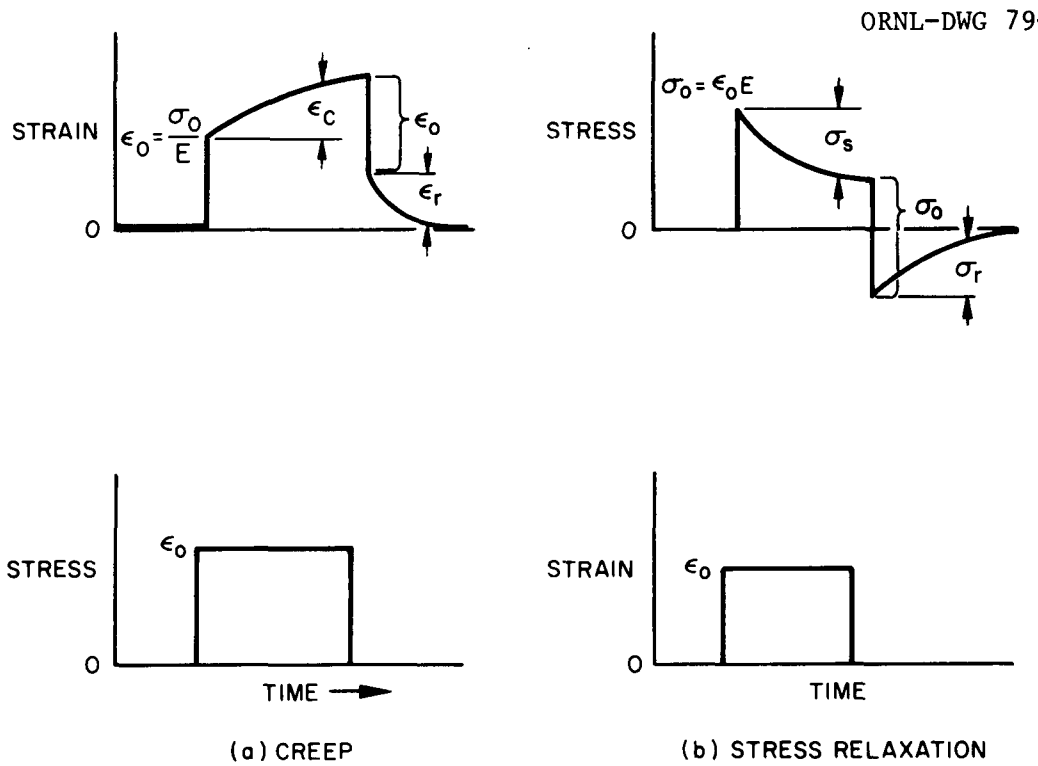

Fig. 3. Comparison Between Creep and Stress Relaxation.

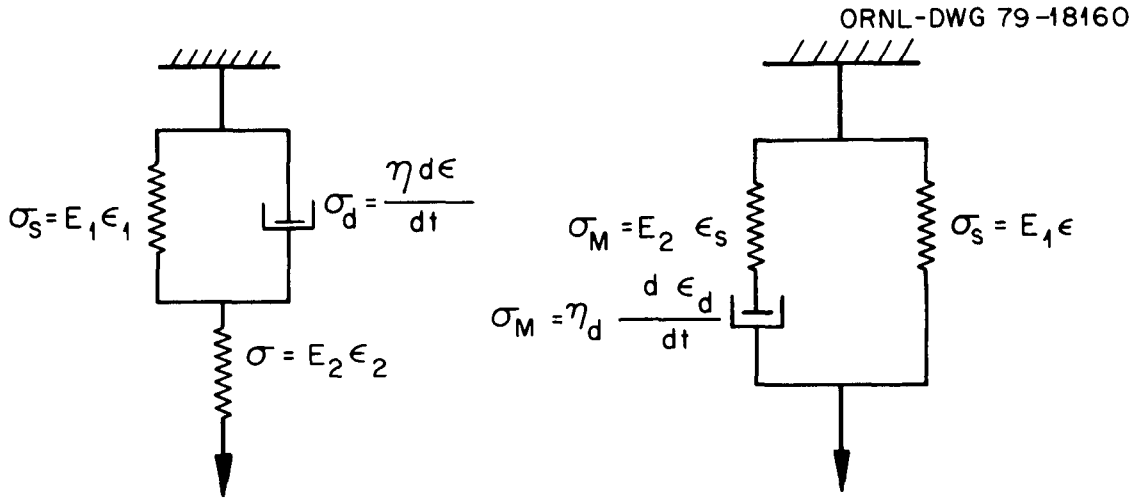

(a) THREE ELEMENT MODEL CONTAINING A VOIGHT UNIT

(b) THREE ELEMENT MODEL CONTAINING A MAXWELL UNIT

Fig. 4. Two Equivalent Models of the Standard Linear Solid.

the Maxwell-type model [Fig. 4(b)] is more suited for the description of stress relaxation. The mathematics of these two models are presented in Appendix A.

The foregoing description indicates that stress relaxation data can be derived from creep data or vice versa. Nowick and Berry[1] have derived the following implicit relationship between creep and stress relaxation functions:

$$1 = M_U J(t) + \int_0^t J(t - t') \frac{dM(t')}{dt'} dt' \quad , \tag{1}$$

where:

M_U = unrelaxed modulus,

$J(t)$ = creep function $\equiv \frac{\varepsilon(t)}{\sigma_0}$,

σ_0 = initial stress,

$\varepsilon(t)$ = time-dependent strain,

$M(t')$ = stress relaxation function $\equiv \frac{\sigma(t)}{\varepsilon_0}$,

ε_0 = initial strain,

t' = time,

$t > t'$.

This equation relates the creep function $J(t)$ and the stress function $M(t)$, but it does so in such a manner that it is difficult to evaluate one function when the other is known. If creep can be expressed as

$$\dot{\varepsilon} = B\sigma^{n'} , \tag{2}$$

where

$\dot{\varepsilon}$ = strain rate,
B = constant,
σ = stress,
n' = constant,

then the time required to relax the stress from the initial stress σ_i to σ is given by Robinson:[2]

$$t = \frac{1}{B\varepsilon(n' - 1)\sigma^{n'-1}}\left[1 - (\sigma/\sigma_i)^{n'-1}\right]. \tag{3}$$

This equation has been used to describe the results from relaxation tests of steel bolts. No work appears to have been done to develop a similar equation for ceramic materials in either compression or tension. Equation (3) was used for a limited temperature range and limited stress range and caution is suggested in extrapolating beyond these ranges. The relaxation tests used in developing Eq. (3) were usually within the range of transient creep (Stage I), while Eq. (2), which was used to derive Eq. (3), refers to the steady state.

The relationships derived in the Appendix using the spring and dashpot models to describe a linear elastic solid are only valid for systems showing creep recovery or relaxation. Creep results in a nonelastic component that manifests itself as a permanent deformation that is nonrecoverable. Thus, for metals, and presumably for ceramics, this nonrecoverable creep complicates modeling of the process considerably.

During creep of metals, the idealized curve shown in Fig. 5 is usually observed. If a material is stressed for long enough so that Stage II creep

ORNL-DWG 79-18161

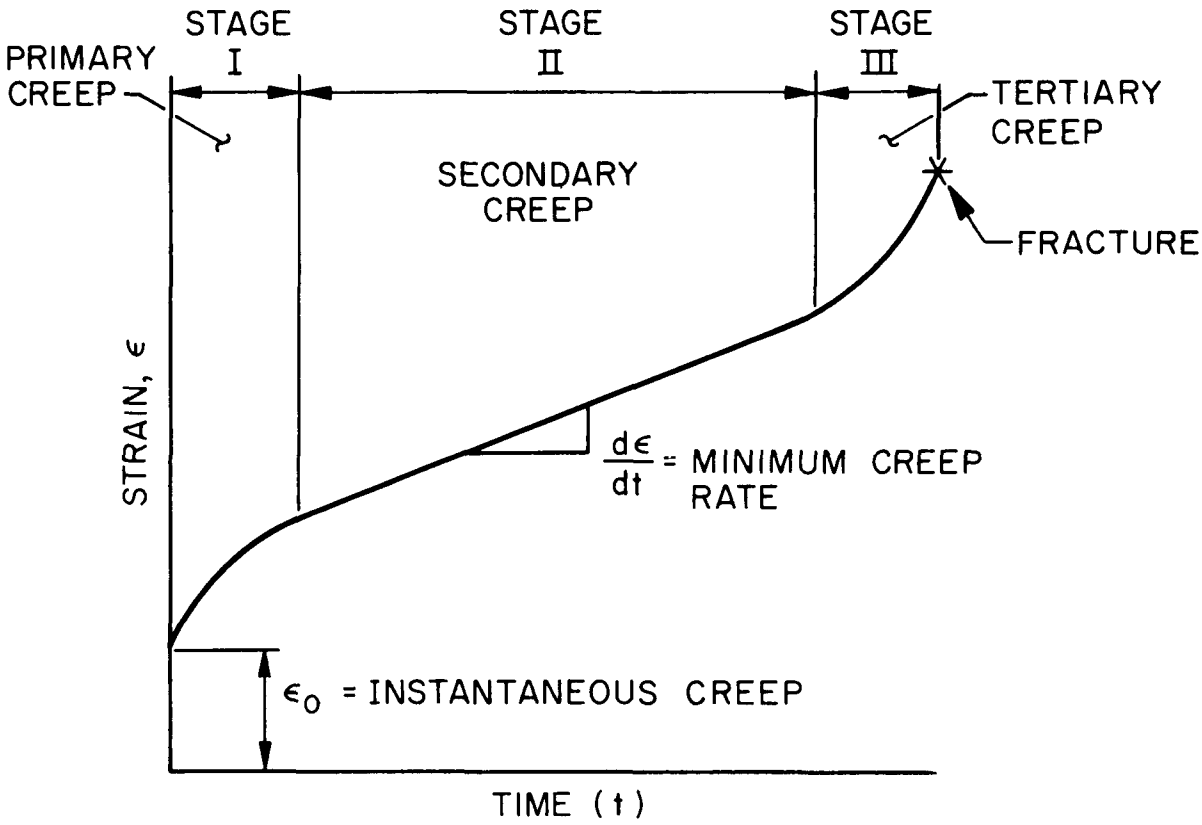

Fig. 5. An Idealized Creep Curve.

is reached and the stress is then removed, the sample will not return to its original dimensions, as suggested in Fig. 3(a), but retains a permanent set or deformation. The curve in Fig. 5 can be broken down further,[3] as shown in Fig. 6. When the creep curve is broken down in this manner, the differences become apparent. The normal creep curve for metals is composed

ORNL-DWG 79-18162

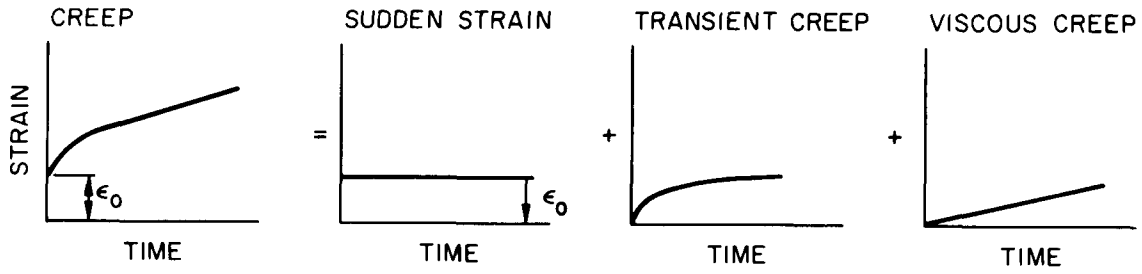

Fig. 6. Competing Processes Contributing to the Creep of Metals.

of three components: sudden strain, transient creep, and viscous creep. The first two are recoverable, while the third is not. Since the viscous creep component is not recoverable, it produces a permanent set or deformation in the material.

In view of the lack of any known explicit correlation between creep and stress relaxation in ceramic materials, we conclude that direct experimental measurement of these properties should be made of structural ceramics considered for use in the HTGR. Furthermore, these tests should be run over a wide range of temperatures and stresses and an attempt made to establish a correlation between these properties.

Creep data are important considering the weight of the HTGR core structure applied to the core support pads. In this case the load is constant so that creep experiments simulate the actual conditions existing in the system. However, during cooldown, especially under emergency conditions, and under core heatup conditions, thermal stresses generated in the ceramics can be quite high. As pointed out by Wei and DiStefano,[4] the ability of the materials to withstand these transients is important to the safety of the core. Under these transient conditions, the strain is constant, or nearly so, and the stresses can be reduced by annealing. These conditions are best simulated by stress relaxation tests.

EXPERIMENTAL METHODS

In general, the two methods commonly used for creep or stress relaxation measurements on ceramic materials are compressive creep tests of cylindrical specimens and three- or four-point bend tests of bars. Compressive creep loading of cylindrical specimens is usually done axially as shown in Fig. 7. In this configuration, stress and strain determinations are relatively straightforward.

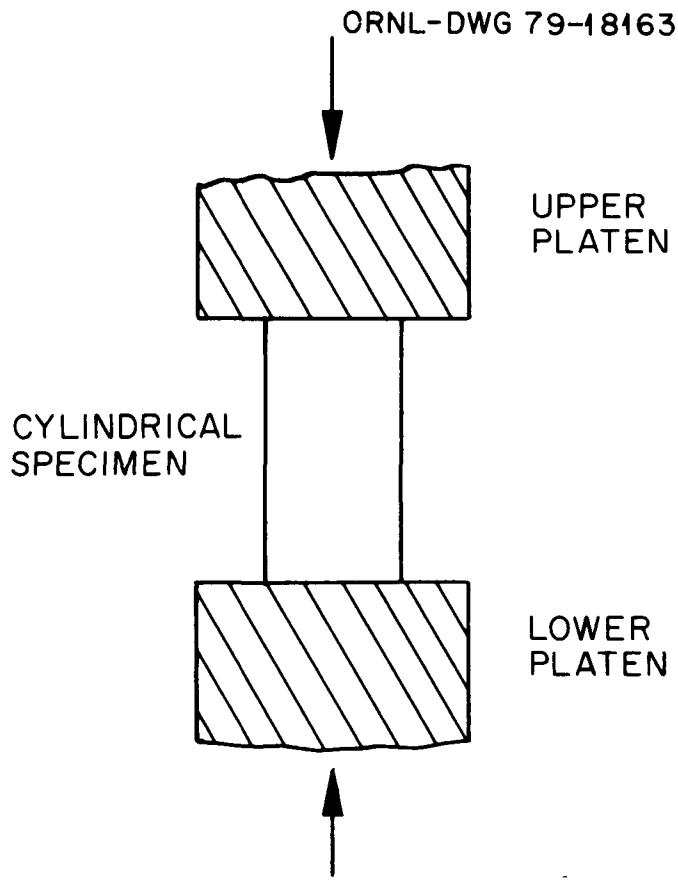

Fig. 7. Schematic of Compression Creep Test.

Creep or stress relaxation measurements using three- and four-point bend tests are somewhat more complicated. These test configurations are shown in Fig. 8. The maximum stress is at the center of the lower surface of the bar in each case. Four-point bending has the advantage of a constant maximum moment over a substantial length of the specimen, (i.e., between the two inner load points), whereas in three-point bending, only a small portion of the specimen is subjected to maximum moment. For this reason the four-point bend test is preferred.

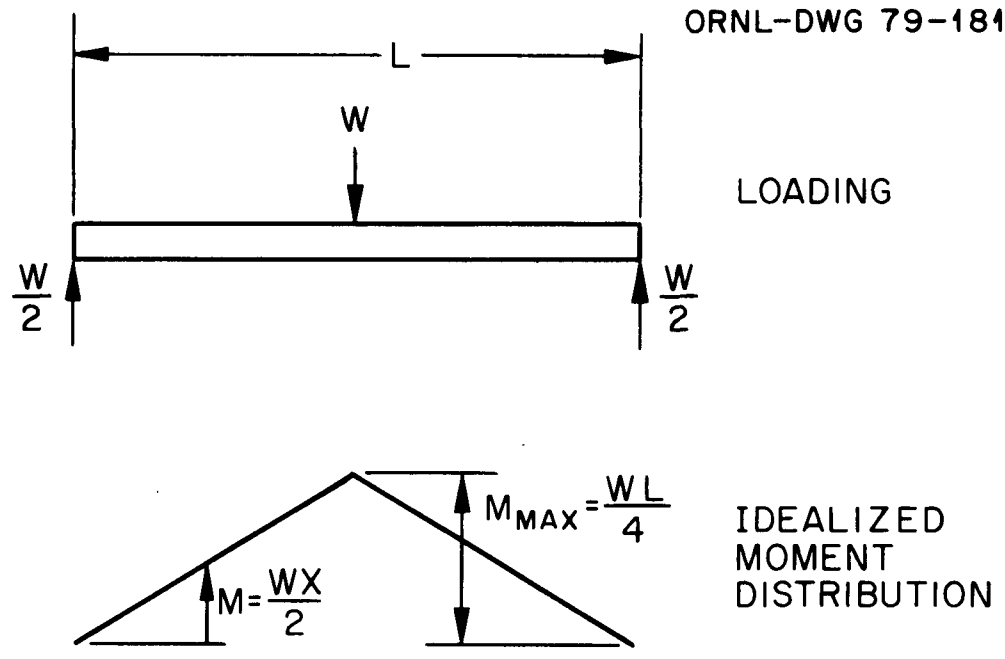

(a) THREE-POINT BEND TEST

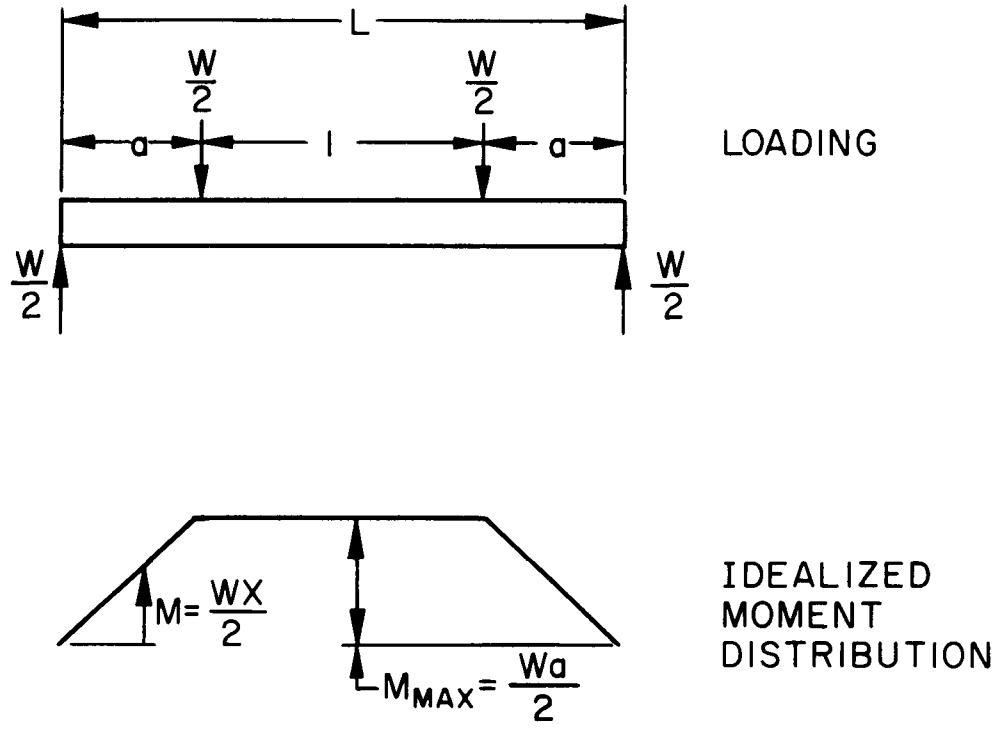

(b) FOUR-POINT BEND TEST

Fig. 8. Schematic of Three- and Four-Point Bend Tests.

In the four-point bend test, the outer fiber stress σ is given as

$$\sigma = \frac{3Wa}{bh^2} , \tag{4}$$

where

W = total applied load,
a = distance between inner and outer load points,
b = width of sample,
h = height of sample.

In the region of constant bending moment, the outer fiber strain ε is determined by

$$\varepsilon = \frac{4h\delta}{\ell^2 + \delta^2} , \tag{5}$$

where δ is deflection at center and ℓ is gauge length (distance between inner load points). The outer fiber strain rate $\dot{\varepsilon}$ is determined by

$$\dot{\varepsilon} = \frac{12h\dot{\delta}}{3L^2 - 4a^2} , \tag{6}$$

where $\dot{\delta}$ is deflection rate at the center of the beam and L is distance between outer loading points.

Sources of Error

Each of these methods has characteristic sources of error where the magnitude is a function of experimental technique. These sources of error are discussed in detail by Rudnick et al,[5] and will only be summarized here.

Compression Test

Conditions that can affect the value of the properties measured in compression include:

1. nonparallel platens,

2. nonparallel ends on test specimens,
3. nonflat ends on test specimens,
4. friction caused by differences in lateral expansion between the specimen and the loading platen,
5. buckling stresses, and
6. end effects.

Four-Point Bend Test

Sources of error in the four-point bend test include:

1. friction forces developed under load points,
2. incorrect spacing of load points and unequal distribution of loads,
3. twisting due to warped specimen or loading fixture,
4. distortion of stresses at inner load points due to wedging, and
5. nonideal material behavior.

Stress Distribution

In the compressive creep test, if the sample is properly prepared, the stress distribution is uniform and perpendicular to the loading direction (i.e., the axis of the cylindrical specimen). However, in the bend tests the stress distribution varies from compression at the top surface to tension at the bottom surface. In addition, deviation of the stress-strain curve from linearity can cause the actual surface stress to differ from the calculated stress, as shown in Fig. 9. Further complications can arise if

ORNL-DWG 79-18165

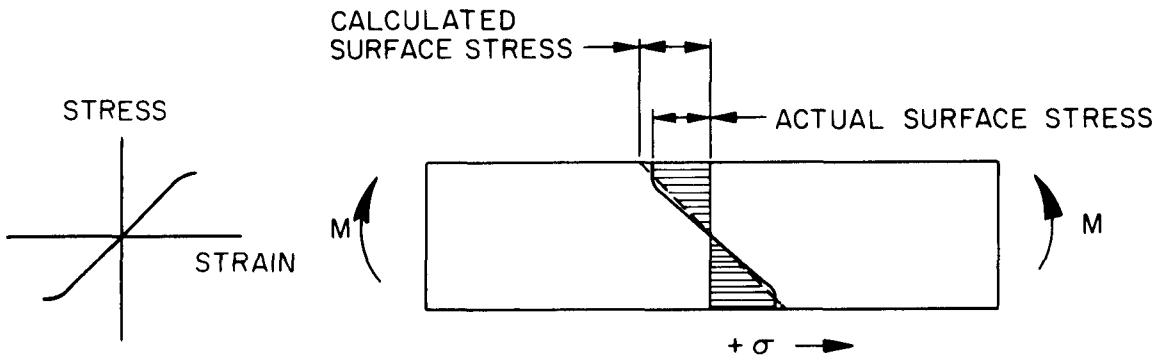

Fig. 9. Effects of Nonlinear Stress-Strain Behavior on Stress Distribution in Bend Test.

the material is nonlinear in the tension region but not in the compression region. In this case the neutral axis will shift toward the compression surface.

Strain Measurements

In comparing the compression test with the four-point bend test, their respective sensitivities to strain measurements and load requirements must be compared. The following calculations are made by assuming a cylindrical test specimen 1.27 cm (0.5 in.) in diameter by 1.91 cm (0.75 in.) long and a bend test specimen 5.08 cm (2.0 in.) long by 0.508 cm (0.2 in.) wide, and 0.254 cm (0.1 in.) high. It is also assumed that strain measurement sensitivity is 5.08×10^{-5} cm (2.0×10^{-5} in.) and the stress requirement is 34.5 MPa (5000 psi).

Compression Test

$$\text{Strain sensitivity} = \frac{\text{minimum measurable strain}}{\text{gage length}}$$

$$= \frac{5.08 \times 10^{-5} \text{ cm}}{1.91 \text{ cm}}$$

$$= 2.66 \times 10^{-5} \text{ cm/cm}$$

$$= 2.66 \times 10^{-3}\% \text{ strain}$$

Load requirement

$$\text{Load} = \text{stress} \times \text{area}$$

$$W = sA$$

$$= 34.5 \times 10^{6} \times \text{!} \times \frac{0.0127^2}{4} = 4370.4\text{N}$$

$$= 982.5 \text{ lb.}$$

Four-Point Bend Test

From Eq. (5),

$$\varepsilon = \frac{4h\delta}{\ell^2 + \delta^2},$$

where δ now = minimum measurable strain

$$\text{Strain sensitivity} = \varepsilon = \frac{4 \times 0.254 \times 5.08 \times 10^{-5}}{2.54 + (5.08 \times 10^{-5})^2}$$

$$= 8.0 \times 10^{-6} \text{ cm/cm}$$

$$= 8 \times 10^{-4}\% \text{ strain.}$$

From Eq. (4),

$$\sigma = \frac{3Wa}{bh^2},$$

$$W = \frac{bh}{3a}$$

$$= \frac{34.5 \times 10^6 \times 0.00508 \times 0.00254^2}{3 \times 0.0127}$$

$$= 29.68 \text{ N}$$

$$= 6.67 \text{ lb.}$$

Thus, for the specimen dimensions used, the four-point bend test has a slight advantage in strain sensitivity. For a given stress measurement, a considerably smaller load ($0.0068W$) is required for the four-point bend test than for the compression test. This means that higher precision and accuracy are required in stress determination for the four-point bend test.

SUMMARY OF EXPERIMENTAL WORK

Determination of physical mechanisms of creep and stress relaxation in structural ceramics is particularly difficult and at the present state of development, there are little available data especially for stress relaxation. There seems to be uniform opinion that both phenomena are thermally activated, but the differences stem from the interpretation of the data in terms of actual mechanisms. Numerous variables appear to be responsible for differences in experimental results and the interpretation reported by various workers. Some of these variables are

1. differences in sample preparation,
2. differences in impurity level and type of impurities,[6–10]
3. experimental techniques,

4. density differences,[11]
5. grain size differences,[9–12]
6. variations in stoichiometry,[13,14]
7. stress level.[15]

Table 2 summarizes parametric requirements for the various creep mechanisms.[16] The numerical value of these parameters, of course, assumes

Table 2. Parametric Requirements for Creep Mechanisms at Elevated Temperatures

Mechanism	Grain size Dependence	Stress Exponent n	Controlling Diffusion Mechanism
Stress-directed lattice diffusion (Nabarro-Herring)	$1/d^2$	1	Lattice
Stress-directed grain-boundary diffusion (Coble)	$1/d^3$	1	Grain boundary
Lattice diffusion around grain-boundary ledges	$1/d$	1	Lattice
Grain-boundary diffusion around grain-boundary ledges	$1/d$	1	Grain boundary
Viscous flow of second phase	$1/d$	1	Second phase
Dislocation climb/glide controlled by climb	0	4.5	Lattice
Dislocation climb/glide controlled by glide	0	3	Lattice
Dissolution of dislocation dipoles	0	5	Pipe
Dissolution of dislocation loops	0	4	Lattice
Dislocations as sources and sinks for vacancies	0	3	Lattice
Pipe diffusion along dislocation cores	0	5	Pipe
Grain-boundary sliding by dislocation glide/climb in zone near boundary	$1/d$	2	Lattice
Grain-broundary sliding by dislocation glide/climb along boundary	$1/d$	2	Grain boundary
Grain-boundary sliding with elongation	$1/d$, $1/d^2$	1	Grain boundary
Grain-boundary sliding without elongation	$1/d^3$	1	Grain boundary

that only one particular process is operating at any one time. This may not necessarily be the case, so experimental data may not always fit these parametric model requirements exactly. Although a given mechanism may be rate controlling, other mechanisms may be occurring simultaneously which could affect the strain rate by causing the apparent parameter values to deviate from the ideal case.

The parameters indicated for the stress-directed grain-boundary diffusion mechanism (Coble creep) are identical to those for grain-boundary sliding with no elongation. The differences between these two lie in a numerical factor, which is $\approx 47 \times 10^{-7}$ in the former case and $\approx 40 \times 10^{-7}$ in the latter.[17] In view of the experimental difficulties with such measurements, this difference may be difficult to detect.

Creep

Most mechanistic determinations have been carried out using creep studies. A summary of available data is given in Table 3. As may be seen in this table, the parameters determined for a given structural ceramic can vary considerably, as does the proposed mechanism. For BeO, creep in tension was found to be the same as that in compression.[18,19] This conclusion was also reached for silicon nitride.[29]

The influence of impurities, or second-phase particles, is somewhat unclear. According to Table 2, second phases can be rate controlling in the case of viscous flow of a second phase. Only one reference indicated any such correlation.[34] In this case the activation energy and the linear stress dependence of the secondary creep rates, supplemented by microstructural analysis, suggested that grain-boundary sliding was controlled by diffusion of zirconium and yttrium cations in the boundary second phase.

Chang[10] discusses the effect of solute atoms on the grain-boundary viscosity and concludes that the effect of adding solute atoms to BeO and Al_2O_3 is to decrease the grain-boundary viscosity, enhance grain-boundary mobility, and thus influence the high-temperature fracture behavior. Cracks caused by the migration of vacancies to the tips of embryonic microcracks become rounded because of atomic migration on the internal surfaces of the cavities. Thus, additives that decrease grain-boundary viscosity delay crack growth and permit more crystalline slip.

Table 3. Summary of Creep Data for Ceramic Materials

Material	Activation Energy (kJ/mole)	Stress Exponent n	Grain Size Dependence $f(d)$	Reference	Mechanism
Al_2O_3	837	1		10	Nabarro-Herring creep
Al_2O_3	597	Low stress 1 High stress 2		15	Low stress: Nabarro-Herring creep
Al_2O_3	482	Low density 2 High density 1		11	Low density: Grain boundary sliding High density: Nabarro-Herring creep
Al_2O_3	Coarse grain 775 Fine grain 544	4 1	0 $1/d^2$	18	Dislocation movement or glide Nabarro-Herring creep
BeO	414	1	$1/d^2$	19	Nabarro-Herring creep
BeO	402	1		20	Nabarro-Herring creep
BeO	502	1		10	Nabarro-Herring creep
MgO	310	1		21	Nabarro-Herring creep
MgO	184	1	T >1300°C $1/d^2$ T <1300°C $1/d^3$	6	Coble creep
MgO		1		22	Nabarro-Herring creep
MgO	214	3.3	0	23	Dislocation motion (climb in absence of glide)
MgO	465	2.6		24	Grain-boundary sliding
MgO	226	Large grain 1 Fine grain 1.5	$1/d^{2.5}$	12	Vacancy formation creep mechanism
MgO			0	25	Grain-boundary sliding + grain-boundary diffusion at triple points
MgO	452	3	0	26,27	Diffusion-controlled growth of the three-dimensional network within subgrains to generate dislocation links that act as dislocation sources
Si_3N_4	586	1.7		28	Grain-broundary sliding accommodated by void deformation at triple points and by some dislocation climb and/or glide
Si_3N_4	649	Compression = 2 Tension > 3		29	Grain-boundary sliding controlled by formation of microcracks
ThO_2	469	1.04–1.59		30	Grain-boundary sliding with grain-boundary pores – diffusion controlled
UO_2	377 Low stress 553 High stress	4.5	$1/d^2$	32	Stress-enhanced diffusion, dislocation motion, grain-boundary sliding
UO_2	364	4.23	0	31	Dislocation motion (exact mechanism indeterminate)
UC	377	3		13	Controlled by self-diffusion of U in UC (hyperstoichiometric UC)
UC	188	1		14	Controlled by diffusion of carbon vacancies (hypostoichiometric UC)
ZrO_2	381–414	1	$1/d$	8	Cation diffusion
ZrO_2	394	1	$1/d$	33	Cation diffusion associated with grain-boundary sliding (CaO stabilized)
ZrO_2	Coarse grain 373 Fine grain 310	1.5	$1/d^2$	9	(Sc_2O_3 doped) mixed mechanism of grain-boundary sliding and local (Sc_2O_3 doped) propagation of intercrystalline cracks
	360	Low stress 1 High stress 6	$1/d^2$		(Y_2O_3 doped) cation diffusion-controlled grain-boundary sliding (Y_2O_3 doped) local propagation of intercrystalline cracks
ZrO_2	460	1		34	Grain-boundary sliding controlled by cation diffusion in a boundary second phase

Impurities, however, seem to affect the creep of ceramic materials in other ways. One consequence of impurities is that they tend to reduce grain growth in the case of magnesia.[7] This serves to accentuate the processes controlled by grain-boundary diffusion. A second consequence of impurities is that they tend to promote viscous (diffusional) creep by suppressing nonviscous (dislocation) contributions to creep through the pinning dislocations.[6,7]

Stress Relaxation

Work has been done to a lesser extent on stress relaxation in ceramic materials; results are summarized in Table 4. For BeO, the activation energies for creep and stress relaxation are virtually identical.

Table 4. Summary of Stress Relaxation Data for Ceramic Materials

Material	Activation Energy (kJ/mole)	Stress Exponent n	Grain size Dependence $f(d)$	Reference	Mechanism
BeO	419		$1/d^3$	35	Grain-boundary sliding
UO_2	385	4.5–20		36	As temperature increases: dislocation glide; dislocation climb and glide and grain-boundary sliding; grain-boundary deformation
UC				37	Thermally activated dislocation mechanism
UC	157	4–6		38	Either Hirsch-Mott hypothesis of jog hardening or long-range stress hypothesis due to dislocation tangles

However, no stress dependence was reported for stress relaxation,[22] and the mechanism is attributed to grain-boundary sliding, compared to the Nabarro-Herring mechanism for creep.[18] A slightly better correlation for the two processes has been reported for UO_2. The activation energies and the stress exponents are similar. The proposed mechanism is undetermined. For UC, dislocation mechanisms are suggested for stress relaxation and diffusion mechanisms are suggested for creep. In the latter, the activation energy and subsequent diffusing species are dependent upon the stoichiometry of the material. Creep in hypostoichiometric UC is controlled by diffusion of carbon vacancies, while creep in hyperstoichiometric UC is controlled by self-diffusion of uranium atoms.

SUMMARY

From this work we conclude that in view of the lack of a demonstrated explicit relationship between creep and stress relaxation in structural ceramic materials, it is necessary to experimentally determine both properties for candidate materials considered for use in HTGR structural

components. Quantitative determinations of both these properties are necessary in order to provide data required for the safety analysis of the effect of stress and temperature transients on the ceramic components. In addition, since little is known about the derivation of stress relaxation data from creep data or vice versa, a serious attempt should be made to determine whether such a relationship exists and, if it does, the conditions under which it is obeyed.

ACKNOWLEDGMENTS

The authors wish to acknowledge the contributions of the following members of the Metals and Ceramics Division: K. Wyatt for typing the original manuscript; C. S. Yust and H. E. McCoy, Jr., for technical review; and A. Rice for final typing. We also wish to acknowledge M. Sheldon of Technical Publications for editing the manuscript.

REFERENCES

1. A. S. Nowick and B. S. Berry, *Anelastic Relaxation in Crystalline Solids*, Academic Press, New York, 1972.
2. E. L. Robinson, "The Resistance to Relaxation of Materials at High Temperature," *Trans. ASME*, 543–54 (1939).
3. E. N. Da C. Andrade, "The Flow in Metals Under Large Constant Stresses," *Proc. (London) Royal Soc.* 90A: 329–42 (1914); quoted in G. E. Dieter, Jr., *Mechanical Metallurgy*, McGraw-Hill, New York, 1961, p. 338.
4. G. C. Wei and J. R. DiStefano, *Safety Status of HTGR Structural Ceramics*, ORNL/TM-5680 (October 1977).
5. A. Rudnick et al., *The Evaluation and Interpretation of Mechanical Properties of Brittle Materials*, AFML-TR-67-361 (DCIC 68-3) (April 1968).
6. R. S. Gordon and G. R. Terwilliger, "Transient Creep in Fe-Doped Polycrystalline MgO," *J. Am. Ceram. Soc.* 55(9): 450–55 (September 1972).

7. T. Zisner and H. Tagai, "High-Temperature Creep of Polycrystalline Magnesia: II. Effects of Additives," *J. Am. Ceram. Soc.* 51(6): 310–14 (June 1968).

8. R. G. St-Jacques and R. Angers, "The Effect of CaO-Concentration on the Creep of CaO-Stabilized ZrO_2," *Trans. J. Brit. Ceram. Soc.* 72(6): 285–89 (June 1973).

9. P. E. Evans, "Creep in Yttria and Scandia – Stabilized Zirconia," *J. Am. Ceram. Soc.* 53(7): 365–69 (July 1970).

10. R. Chang, "High Temperatute Creep and Anelastic Phenomena in Polycrystalline Refractory Oxides," *J. Nucl. Mater.* 2: 174–81 (1959).

11. G. M. Fryer and P. Thompson, "Compressive Creep of Porous Polycrystalline Alumina," *Trans. J. Brit. Ceram. Soc.* 72(6): 61–66 (1973).

12. E. M. Passmore, R. H. Duff, and T. Vasilos, "Creep of Dense Polycrystalline Magnesium Oxide," *J. Am. Ceram. Soc.* 49(1): 594–600 (November 1966).

13. D. E. Stellrecht, M. S. Farkas, and D. P. Doak, "Compressive Creep of Uranium Carbide," *J. Am. Ceram. Soc.* 51(8): 455–58 (August 1968).

14. N. M. Killey, "The Secondary Creep Behavior of Uranium Monocarbide in Compression I: Hypostoichiometric Uranium Monocarbide,: *J. Nucl. Mater.* 41: 178–86 (1971).

15. E. M. Passmore and T. Vasilos, "Creep of the Dense, Pure, Fine-Grained Aluminum Oxide," *J. Am. Ceram. Soc.* 49(3): 166–68 (March 1966).

16. T. G. Langdon, D. R. Cropper, and J. A. Pask, "Creep Mechanisms in Ceramic Materials at Elevated Temperatures," pp. 297–313 in *Materials Science Research*, Vol. 5, ed. by W. W. Kriegel and H. Palmour, III, Plenum Press, New York, 1971.

17. R. D. Gifkins, "Diffusional Creep Mechanisms," *J. Am. Ceram. Soc.* 51(2): 69–72 (February 1968).

18. S. I. Warshaw and F. H. Norton, "Deformation Behavior of Polycrystalline Aluminum Oxide," *J. Am. Ceram. Soc.* 45(10): 479–86 (October 1962).

19. W. L. Barmore and R. R. Vandervoort, "High Temperature Plastic Deformation of Polycrystalline Beryllium Oxide," *J. Am. Ceram. Soc.* 48(10): 499–505 (October 1965).

20. R. R. Vandervoort and W. L. Barmore, "Compressive Creep of Polycrystalline Beryllium Oxide," *J. Am. Ceram. Soc.* 46(4): 180–84 (April 1963).

21. T. Vasilos, J. B. Mitchell, and R. M. Spriggs, "Creep of Polycrystalline Magnesia," *J. Am. Ceram. Soc.* 47(4): 203–04 (April 1964).

22. H. Tagai and T. Zisner, "High Temperature Creep of Polycrystalline Magnesia: I. Effect of Simultaneous Grain Growth," *J. Am. Ceram. Soc.* 51(6): 303–10 (June 1968).

23. T. G. Langdon and J. A. Pask, "The Mechanism of Creep in Polycrystalline Magnesium Oxide," *Acta Met.* 18: 505–10 (May 1970).

24. J. H. Hensler and G. V. Cullen, "Stress, Temperature, and Strain Rate in Creep of Magnesium Oxide," *J. Am. Ceram. Soc.* 51(10): 557–59 (October 1968).

25. J. H. Hensler and G. V. Cullen, "Grain Shape Change During Creep in Magnesium Oxide," *J. Am. Ceram. Soc.* 50(11): 584–85 (November 1967).

26. J. M. Birch and B. Wilshire, "Deformation Processes During High Temperature Creep of Single and Polycrystalline MgO," *Proc. Brit. Ceram. Soc.* 25: 127–38 (May 1975).

27. J. M. Birch and B. Wilshire, "Work Hardening and Recovery During Compressive Creep of Polycrystalline MgO," *J. Mater. Sci.* 9: 794–800 (1974).

28. S. U. Din and P. S. Nicholson, "Creep of Hot-Pressed Silicon Nitride," *J. Mater. Sci.* 10: 1375–80 (1975).

29. J. M. Birch, B. Wilshire, and D. J. Godfrey, "Deformation and Fracture Processes During Creep of Reaction Bonded and Hot Pressed Silicon Nitride," *Proc. Brit. Ceram. Soc.* 26: 141–54 (July 1978).

30. L. E. Poteat and C. S. Yust, "Creep of Polycrystalline Thorium Dioxide," *J. Am. Ceram. Soc.* 49(8): 410–14 (August 1966).

31. R. E. Canon, J.T.A. Roberts, and R. J. Beals, "Deformation of UO_2 at High Temperatures," *J. Am. Ceram. Soc.* 54(2): 105–12 (February 1971).

32. P. E. Bohaboy, R. R. Asamoto, and A. E. Conti, *Compressive Creep Characteristics of Stoichiometric Uranium Dioxide*, GEAP-10054 (May 1969).

33. R. G. St-Jacques and R. Angers, "Creep of CaO-Stabilized ZrO_2," *J. Am. Ceram. Soc.* 55(11): 571–74 (November 1972).

34. L. L. Fehrenbacher, F. P. Bailey, and N. A. McKinnon, "Compressive Creep of Yttria Rare Earth Stabilized Zirconia Storage Heater Refractories," *SAMPE Quart.* 2: 18–30 (1971).

35. D. G. Walker, W. B. Rotsey, and B.R.A. Wood, "Stress Relaxation in Beryllia," *J. Mater. Sci.* 6: 281–88 (1971).

36. J.T.A. Roberts, "Mechanical Equation of State and High-Temperature Deformation ($\geq$0.5 T_m) of Uranium Dioxide," *Acta Met.* 22: 873–78 (July 1974).

37. J. L. Routbort, "High Temperature Deformation of Polycrystalline Uranium Carbide," *J. Nucl. Mater.* 44: 24–30 (1972).

38. R. Chang, "Flow and Recovery Properties of Nearly Stoichiometric Polycrystalline Uranium Carbide and the Mechanism of Work Hardening of Crystalline Solids," *J. Appl. Phys.* 33(3): 858–63 (March 1962).

APPENDIX

The derivation of the mathematical relationship for the spring and dashpot models has been presented in numerous references and will be summarized here. The elements of these models are the spring and the dashpot, shown schematically in Fig. A1. The spring model represents a

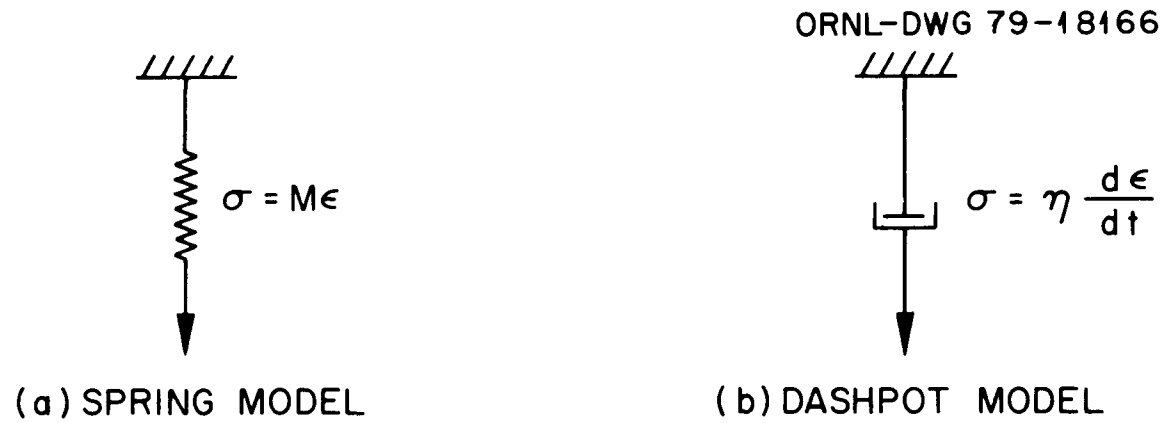

Fig. A1. Schematic of Spring and Dashpot Models.

linear-elastic solid, so that

$$\sigma = M\varepsilon = \varepsilon/J \ , \tag{A1}$$

where

σ = stress,
ε = strain,
M = modulus,
J = $1/M$ = compliance,

that is, Hooke's law is obeyed perfectly. The dashpot, on the other hand, has a viscous coefficient η such that

$$\sigma = \eta \frac{d\varepsilon}{dt} \ . \tag{A2}$$

According to Eq. (A2) the strain is not recoverable upon release of the stress when the dashpot is used alone.

These simple models can be extended further by placing them in series or in parallel. When placed in series (Fig. A2), the resulting two-parameter model is called the Maxwell model. The response of this model to

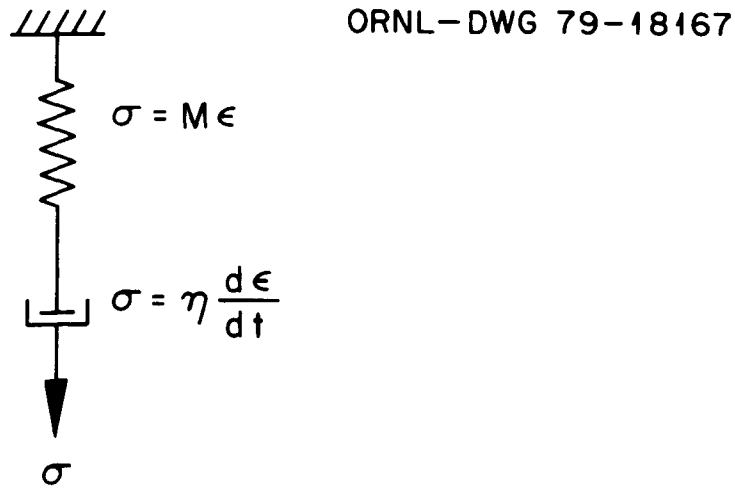

Fig. A2. The Maxwell Model.

the application of a load (creep) is shown in Fig. A3. The Maxwell model is capable of stress relaxation. If the system is subjected to a constant

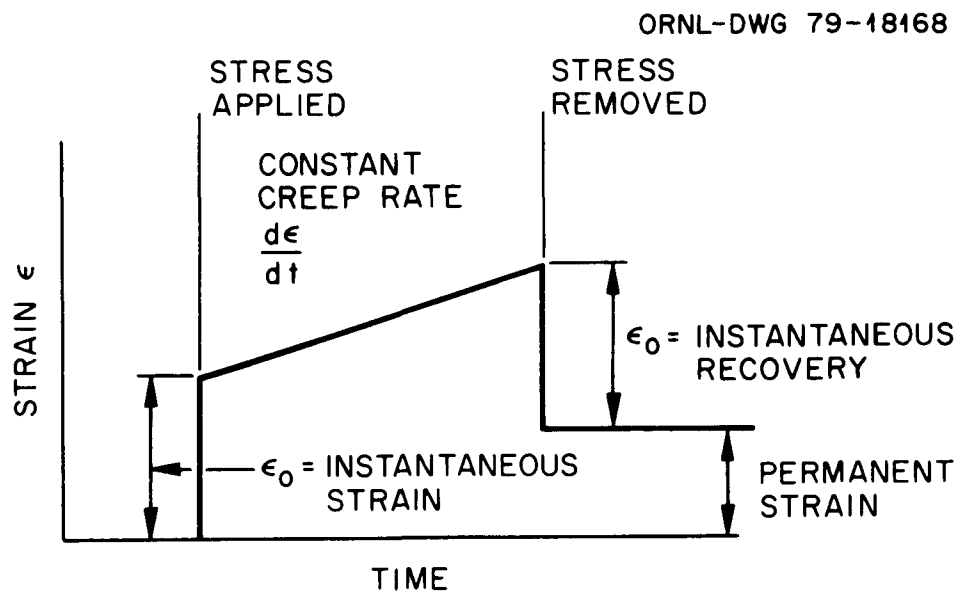

Fig. A3. Response of the Maxwell Model to Application of a Load.

strain ε_0, at $t = 0$, there is an instantaneous stress σ_0, on the spring, since the dashpot will not yield instantaneously. With increasing time the dashpot will continue to flow in accordance with Eq. (A2) and the stress on the dashpot and the spring will go to zero. However, this model does not demonstrate creep recovery.

When the spring and dashpot are placed in parallel (Fig. A4), the

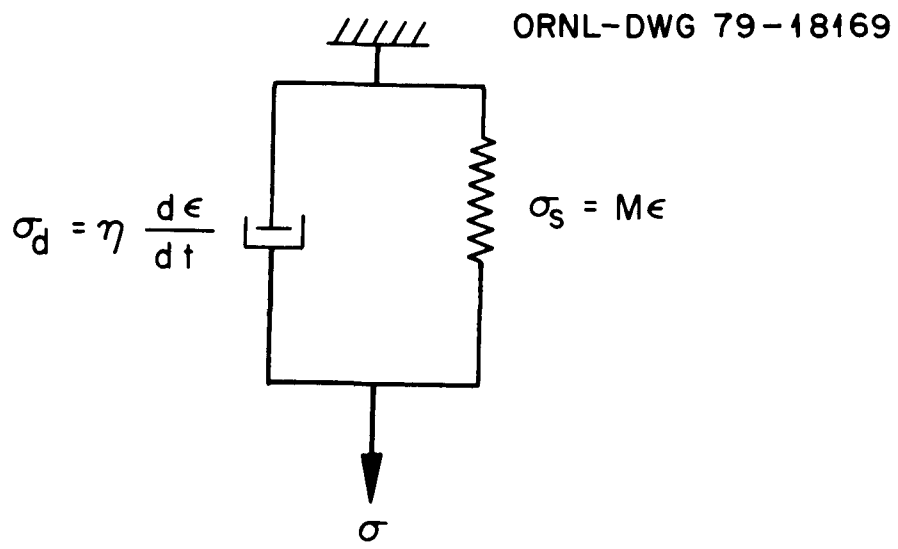

Fig. A4. The Voight (or Kelvin) Model.

unit is called the Kelvin or Voight model. In this system:

$$\sigma = \sigma_d + \sigma_s \ , \tag{A3}$$

where σ_d and σ_s are defined by Eqs. (A1) and (A2). From Eq. (A2)

$$\frac{d\varepsilon}{dt} = \frac{\sigma_d}{\eta} \ . \tag{A4}$$

Substituting Eq. (A-3) into Eq. (A4) yields

$$\frac{d\varepsilon}{dt} = \frac{\sigma - \sigma s}{\eta} \tag{A5}$$

and substituting Eq. (A1) into Eq. (A5) gives

$$\frac{d\epsilon}{dt} = \frac{\sigma - M\epsilon}{\eta} \quad . \tag{A6}$$

This relationship is illustrated in Fig. A-5, which shows that the model demonstrates creep and creep recovery but not instantaneous recovery or extension.

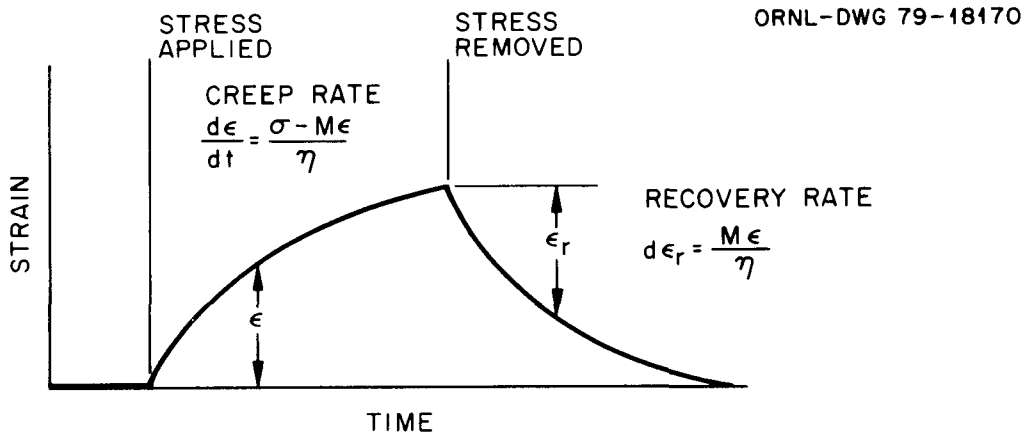

Fig. A5. Response of the Voight Model to Application of a Load.

The Maxwell model demonstrates all the experimentally observed creep features except creep recovery, while the Voight model demonstrates all the features of instantaneous extension and recovery. In order to more completely describe experimental behavior of most solid materials at high temperatures, a three-element model appears to be necessary.

Two different three-element models are described, one containing a Voight unit and one containing a Maxwell unit (Fig. A6). The model with a Voight unit consists of a spring in series with the Voight unit. This combination will impart an instantaneous strain to the two-element Voight model and thus overcome the objections to that model. On the other hand, the model containing a Maxwell unit consists of a spring in parallel with the Maxwell unit. This spring applies a force to the dashpot upon release of the stress and allows the model to demonstrate creep recovery, thus overcoming the objections to the Maxwell model.

ORNL-DWG 79-18171

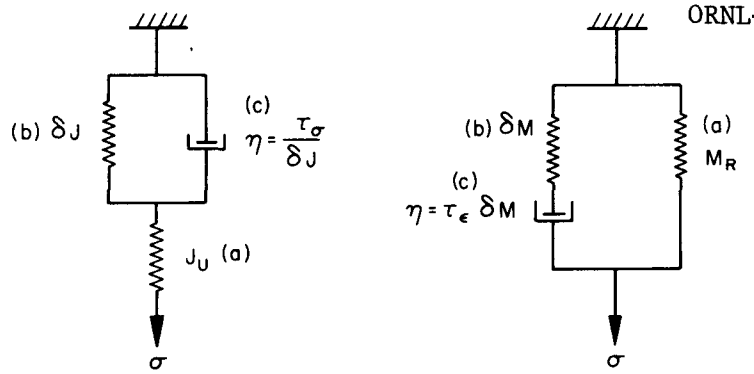

(a) THREE ELEMENT MODEL CONTAINING A VOIGHT UNIT

(b) THREE ELEMENT MODEL CONTAINING A MAXWELL UNIT

Fig. A6. Three-Element Models of a Standard Linear Solid.

In order to derive the differential stress-strain equation for these two models, it is convenient to define several terms and to discuss creep in terms of compliance and stress relaxation in terms of the modulus, as shown in Fig. A7. The quantity J_U is called the unrelaxed compliance

ORNL-DWG 79-18172

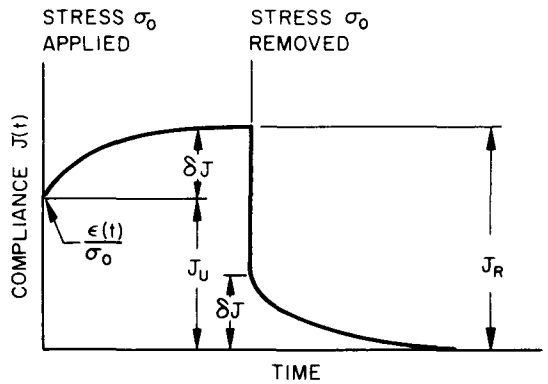

CREEP OF LINEAR ELASTIC SOLID

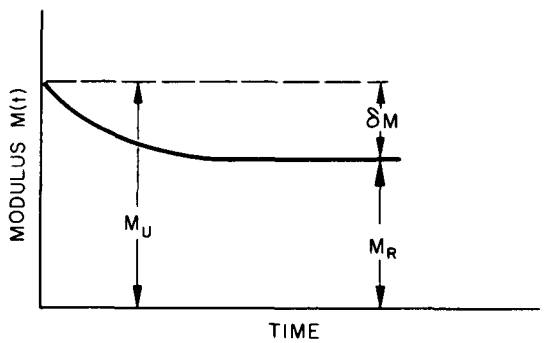

Fig. A7. Comparison of Creep and Stress Relaxation in a Linear Elastic Solid.

since it is a measure of the deformation before relaxation takes place. The equilibrium value of the compliance after relaxation is called the relaxed compliance, J_R, and the difference between these two values is the relaxation of the compliance δJ. By definition,

$$J(0) \equiv J_U \ , \tag{A7}$$

$$J(\infty) \equiv J_R \ , \tag{A8}$$

$$\delta J \equiv J_R - J_U \ . \tag{A9}$$

For stress relaxation, it is convenient to use the modulus values shown in Fig. A7. At $t = 0$ the value of the modulus is called the unrelaxed modulus M_U and after a period of time the equilibrium value of the modulus is the relaxed modulus M_R. Again, the difference is called the relaxation of the modulus δM. Thus,

$$M(0) \equiv M_U \ , \tag{A10}$$

$$M(\infty) \equiv M_R \ , \tag{A11}$$

$$(M_U - M_R) \equiv \delta M \ . \tag{A12}$$

In view of the prior definitions, the following relationships can be shown to be true:

$$M_R = 1/J_R \ , \tag{A13}$$

$$M_U = 1/J_U \ , \tag{A14}$$

$$\delta M = \delta J/J_U J_R \ . \tag{A15}$$

From Fig. A6(a), it can be seen that $\varepsilon_a = J_U \sigma_a$, $\varepsilon_b = \delta J \sigma_b$, and $\dot{\varepsilon} = \delta J \sigma_c / \tau_\sigma$.

Also,

$$\varepsilon = \varepsilon_a + \varepsilon_b, \quad \varepsilon_b = \varepsilon_c ,$$

$$\sigma = \sigma_a = \sigma_b + \sigma_c ,$$

and

$$\frac{1}{J_U}\varepsilon_a = \frac{1}{\delta J}(\varepsilon_b + \tau_\sigma \dot{\varepsilon}) . \tag{A16}$$

From Eq. (A9) and rearranging terms,

$$(J_R - J_U)\varepsilon_a = J_U\varepsilon_b + \tau_\sigma \dot{\varepsilon}_c J_U ,$$

$$J_R\varepsilon_a - J_U\varepsilon_a = J_U\varepsilon_b + \tau_\sigma \dot{\varepsilon} J_U ,$$

$$J_R\varepsilon_a = (J_U\varepsilon_a + J_U\varepsilon_b) + \tau_\sigma \dot{\varepsilon} J_U ,$$

$$J_R\varepsilon_a = J_U\varepsilon + \tau_\sigma \dot{\varepsilon} J_U . \tag{A17}$$

Dividing Eq. (A17) by J_U gives

$$\frac{J_R\varepsilon_a}{J_U} = \varepsilon + \tau_\sigma \dot{\varepsilon}_c .$$

But, since

$$\sigma = \frac{\varepsilon_a}{J_U} ,$$

$$J_R\sigma = \varepsilon + \tau_\sigma \dot{\varepsilon}_c , \tag{A18}$$

$$\varepsilon_c = \varepsilon - \varepsilon_a = \varepsilon - J_U\sigma_a = \varepsilon - J_U\sigma .$$

Therefore

$$\dot{\varepsilon}_c = \dot{\varepsilon} - J_U\dot{\sigma} \ . \tag{A19}$$

Substituting Eq. (A19) into Eq. (A18) gives

$$J_R\sigma = \varepsilon + \tau_\sigma\dot{\varepsilon} - \tau_\sigma J_U\dot{\sigma} \ ,$$

$$\sigma + \frac{\tau_\sigma J_U\dot{\sigma}}{J_R} = \frac{\varepsilon}{J_R} + \frac{\tau_\sigma\dot{\varepsilon}}{J_R} \ , \tag{A20}$$

$$\sigma = \tau_\varepsilon\dot{\sigma} = \frac{\varepsilon}{J_R} + \frac{\tau_\varepsilon\dot{\varepsilon}}{J_U} \ ,$$

where $\tau\varepsilon \equiv \tau\sigma J_U/J_R$.

A similar procedure can be followed to derive the differential stress-strain equation for the three-element model containing a Maxwell unit [Fig. A6(b)]. From Fig. A6(b) we have

$$\sigma_a = M_R\varepsilon_a \ , \ \sigma_b = \delta M\varepsilon_b \ , \ \sigma_c = \tau_\varepsilon\delta M\dot{\varepsilon}_c$$

and

$$\sigma = \sigma_a + \sigma_b \ , \ \sigma_b = \sigma_c \ , \tag{A21}$$

$$\varepsilon = \varepsilon_a = \varepsilon_b + \varepsilon_c \ . \tag{A22}$$

Therefore, from Eq. (A21)

$$\sigma = \sigma_a + \sigma_b = M_R\varepsilon_a + \tau_\varepsilon\delta M\dot{\varepsilon}_c \ ,$$

$$= M_R\varepsilon + \tau_\varepsilon\delta M\dot{\varepsilon}_c \ . \tag{A23}$$

From Eq. (A22)

$$\varepsilon_c = \varepsilon - \varepsilon_b = \varepsilon - \sigma_b/\delta M \ ,$$

$$\dot{\varepsilon} = \dot{\varepsilon} - \frac{\dot{\sigma}_b}{\delta M} \ , \tag{A24}$$

$$\sigma_b = \sigma - \sigma_a = \sigma - M_R\varepsilon \ ,$$

$$\dot{\sigma}_b = \dot{\sigma} - M_R\dot{\varepsilon} \ . \tag{A25}$$

Substituting Eq. (A25) into Eq. (A24) gives

$$\dot{\varepsilon}_c = \dot{\varepsilon} - \frac{(\dot{\sigma} - M_R\dot{\varepsilon})}{\delta M} \ . \tag{A26}$$

Substituting Eq. (A26) into Eq. (A23) gives

$$\sigma = M_R\varepsilon + \tau_\varepsilon \delta M\dot{\varepsilon} - \tau_\varepsilon\dot{\sigma} + \tau_\varepsilon M_R\dot{\varepsilon} \ ,$$

$$\sigma + \tau_\varepsilon\dot{\sigma} = M_R\varepsilon + \tau_\varepsilon\dot{\varepsilon}(\delta M + M_R) \ .$$

From Eq. (A12),

$$\sigma + \tau_\varepsilon\dot{\sigma} = M_R\varepsilon + \tau_\varepsilon\dot{\varepsilon}M_U \ . \tag{A27}$$

Since $M_R = 1/J_R$, and $M_U = 1/J_U$, Eq. (A27) is identical with Eq. (A20) and the two models yield the same differential stress-strain equation.

REFERENCE

1. A. S. Nowick and B. S. Berry, *Anelastic Relaxation in Crystalline Solids*, Academic Press, New York, 1972.

ORNL/TM-7239
Distribution
Category UC-77

INTERNAL DISTRIBUTION

1–2. Central Research Library
3. Document Reference Section
4–5. Laboratory Records Department
6. Laboratory Records, ORNL RC
7. ORNL Patent Section
8. R. L. Beatty
9. A. J. Caputo
10. G. W. Clark
11. W. A. Coghlan
12. R. G. Donnelly
13. R. E. Helms
14–16. M. R. Hill
17. F. J. Homan
18. R. R. Judkins
19–28. P. R. Kasten
29. J. J. Kurtz
30. W. J. Lackey
31. R. J. Lauf
32. H. E. McCoy
33. C. S. Morgan
34. J. C. Ogle
35. A. E. Pasto
36–40. P. L. Rittenhouse
41. G. C. Robinson
42–46. J. E. Selle
47. G. M. Slaughter
48–52. V. J. Tennery
53. S. M. Tiegs
54. A. L. Bement, Jr. (Consultant)
55. W. R. Hibbard, Jr. (Consultant)
56. E. H. Kottcamp, Jr. (Consultant)
57. Alan Lawley (Consultant)
58. M. J. Mayfield (Consultant)
59. J. T. Stringer (Consultant)

EXTERNAL DISTRIBUTION

60–61. DOE, DIVISION OF NUCLEAR POWER DEVELOPMENT, Washington, DC 20545

Director
G. A. Newby

62. SAN-DEVELOPMENT, SAN DIEGO AREA OFFICE, P.O. Box 81325, San Diego, CA 92138

Senior Program Coordinator

63. DOE, SAN FRANCISCO OPERATIONS OFFICE, 1333 Broadway, Wells Fargo Building, Oakland, CA 94612

Manager

64–65. DOE, OAK RIDGE OPERATIONS OFFICE, P.O. Box E, Oak Ridge, TN 37830

Office of Assistant Manager, Energy Research and Development
Director, Nuclear Research and Development Division

66–231. DOE, TECHNICAL INFORMATION CENTER, P.O. Box 62, Oak Ridge, TN 37830

For distribution as shown in TID-4500 Distribution Category, UC-77 (Gas Cooled Reactor Technology)